nature nanotechnology

Article

https://doi.org/10.1038/s41565-023-01581-2

Valley-centre tandem perovskite light-emitting diodes

Received: 9 March 2023

Accepted: 22 November 2023

Published online: 16 January 2024

Check for updates

Hyeon-Dong Lee[1,5], Seung-Je Woo[1,5], Sungjin Kim[1,5], Junho Kim[2], Huanyu Zhou[1], Shin Jung Han[1], Kyung Yeon Jang[1], Dong-Hyeok Kim[1], Jinwoo Park[1], Seunghyup Yoo[2] & Tae-Woo Lee[1,3,4]

Perovskite light-emitting diodes (PeLEDs) have emerged as a promising new light source for displays. The development roadmap for commercializing PeLEDs should include a tandem device structure, specifically by stacking a thin nanocrystal PeLED unit and an organic light-emitting diode unit, which can achieve a vivid and efficient tandem display; however, simply combining light-emitting diodes with different characteristics does not guarantee both narrowband emission and high efficiency, as it may cause a broadened electroluminescence spectra and a charge imbalance. Here, by conducting optical simulations of the hybrid tandem (h-tandem) PeLED, we have discovered a crucial optical microcavity structure known as the h-tandem valley, which enables the h-tandem PeLED to emit light with a narrow bandwidth. Specifically, the centre structure of the h-tandem valley (we call it valley-centre tandem) demonstrates near-perfect charge balance and optimal microcavity effects. As a result, the h-tandem PeLED achieves a high external quantum efficiency of 37.0% and high colour purity with a narrow full-width at half-maximum of 27.3 nm (versus 64.5 nm in organic light-emitting diodes) along with a fast on–off response. These findings offer a new strategy to overcome the limitations of nanocrystal-based PeLEDs, providing valuable optical and electrical guidelines for integrating different types of light-emitting device into practical display applications.

Perovskite light-emitting diodes (PeLEDs) are promising as the light source for next-generation displays because of the following advantages: (1) high colour saturation due to narrow emission spectra (full-width at half-maximum (FWHM) of ~20 nm), (2) self-emission, (3) facile synthesis, (4) high luminescence efficiency and (5) low material cost[1–5]. The perovskite emitters can fully cover the Rec. 2020 colour space[3] and the efficiency of PeLEDs has been rapidly increased to an external quantum efficiency (EQE) of 28.9% by confining the charge carriers in the perovskite nanocrystal (PNC) and suppressing the formation of defects[6–8]. However, the device efficiency of PeLEDs is still lower than those of the state-of-the-art organic light-emitting diodes (OLEDs)[9–11].

A tandem device structure incorporating two or more device units in series is widely used in optoelectronic devices to increase efficiency[12,13]. There are many advantages in various aspects of applying a tandem structure to light-emitting diodes (LEDs). Tandem LEDs that use a charge generation layer (CGL) could achieve higher EQE by combining the efficiencies of individual light-emitting units. This also results in reduced electrical stress applied to the tandem device compared with the single device to exhibit equivalent brightness, leading

[1]Department of Materials Science and Engineering, Seoul National University, Seoul, Republic of Korea. [2]School of Electrical Engineering, Korea Advanced Institute of Science and Technology (KAIST), Daejeon, Republic of Korea. [3]Institute of Engineering Research, Research Institute of Advanced Materials, Soft Foundry, Seoul National University, Seoul, Republic of Korea. [4]SN Display Co., Ltd., Seoul, Republic of Korea. [5]These authors contributed equally: Hyeon-Dong Lee, Seung-Je Woo, Sungjin Kim. e-mail: twlees@snu.ac.kr

to improved operational lifetime in the tandem device. In addition, by adjusting the microcavity structure of tandem LEDs, the FWHM of the emission spectra of stacked LEDs can be narrowed[14]. For these reasons, single-colour-stacked tandem OLEDs for red, green and blue sub-pixels are emerging as a new standard for next-generation displays in tablets and laptops[15–17].

In this circumstance, a tandem device structure must be considered in the development roadmap for the commercialization of PeLEDs. At the current stage of the roadmap, the most promising strategy for fabricating a tandem PeLED is stacking a thin, optically transparent solution-processed colloidal nanocrystal PeLED unit with a vacuum-deposited OLED unit. The use of a tandem structure incorporating a thin-nanocrystal-film-based PeLED with an OLED can realize a vivid and efficient tandem display by utilizing a well-established manufacturing process of OLEDs. However, simply combining two different types of LED composed of a narrowband PeLED and a broadband OLED that have different current density–voltage–luminance (J–V–L) and electroluminescence (EL) characteristics does not guarantee both narrowband emission and high efficiency in the tandem structure, unlike conventional tandem OLEDs combining the same OLED units. In particular, simply combining different types of emitter with different J–V–L characteristics leads to a broadening and shift in the EL spectra depending on the driving voltage due to charge imbalance.

In this work, we propose a strategy for designing an optically defined cavity device structure for vivid hybrid tandem (h-tandem) PeLEDs and provide an optical and electrical guideline to make the h-tandem structure that can achieve high device efficiency, high colour purity and perfect charge balance. We developed an h-tandem PeLED by combining a pure green PeLED (FWHM = 21.9 nm) and a green phosphorescent OLED (FWHM = 64.5 nm), which show completely different emission spectra (Fig. 1 and Supplementary Figs. 1 and 2). Through the optical simulation of h-tandem PeLED, we discovered a crucial optical microcavity structure (referred to as an h-tandem valley) that produces a narrow FWHM. In particular, with the device structure at the centre of the h-tandem valley, near-perfect charge balance was achieved, leading to extremely high efficiency. The different EL emissions of the PeLED and OLED units were spectrally matched by the fine control of the microcavity structure and resulted in a very narrow FWHM of 27.3 nm of the EL emission of the h-tandem PeLED. The PeLED unit and OLED unit contributed to the efficiency of the h-tandem PeLED without electrical loss due to the near-perfect charge balance, showing a high device efficiency of EQE = 37.0% and current efficiency (CE) = 151.8 cd A^{-1}.

The h-tandem valley: a crucial optical microcavity structure of h-tandem PeLEDs

For developing h-tandem PeLEDs, realizing improved device efficiency along with a narrow EL spectrum is much more complicated than developing typical tandem devices combining the same units. An optically transparent (that is, thin) colloidal nanocrystal PeLED as a stacking unit is more suitable for tandem devices compared with a bulk polycrystalline PeLED that usually employs an emitting layer that is a few hundred nanometres thick[8] because of the strong absorption of emitted light from the top units and difficulty in controlling the charge balance in tandem devices. Because the shape, peak and FWHM of the emission spectra of the PeLED and OLED largely differ, it is important to carefully control the microcavity effect of each unit in the tandem device to realize a narrow EL spectrum of the tandem device (Fig. 1a–e and Supplementary Fig. 2). PeLEDs and OLEDs generally have a weak microcavity structure made of a highly reflective metal electrode and a high-refractive-index indium tin oxide electrode. Depending on the position of the perovskite or organic emitters within the microcavity, the wavelength-dependent emitter–cavity coupling varies, resulting in different outcoupling efficiencies and emission spectra shapes (Supplementary Figs. 2 and 3). By performing an optical simulation of the h-tandem PeLED, we calculated the FWHM of EL emission depending on the thickness of the hole transport layer and electron transport layer (ETL) in the top unit and discovered the h-tandem valley that leads to a narrow FWHM under 28 nm by the well-matched EL spectra of the PeLED and OLED units (Fig. 1f and Supplementary Fig. 3). Then, we fabricated h-tandem PeLEDs with the structure within and outside the h-tandem valley. Here we used a colloidal PNC for the PeLED unit in tandem devices. The device with the structure at the centre of the h-tandem valley (valley-centre tandem) showed an FWHM of 27.3 nm, which perfectly matched with the calculated FWHM of 27.5 nm from optical simulation (Fig. 1c and Supplementary Figs. 3 and 4). On the other hand, the device with the structure outside the h-tandem valley (off-valleys 1 and 2) showed broad FWHMs of 58.5 and 57.0 nm, respectively, as expected from the optical simulation.

In addition, the valley-centre tandem exhibited a high device efficiency of EQE = 37.0% and CE = 151.8 cd A^{-1} without electrical loss due to the near-perfect charge balance. The separated single-unit PeLED and OLED that originates from the tandem device are optimized to achieve the best efficiency of the tandem devices at the optical valley centre. The efficiency of valley-centre tandem was even higher than the sum of the efficiency of a single-unit PeLED (EQE, 14.6%; CE, 66.2 cd A^{-1}) and the efficiency of a single-unit OLED (EQE, 20.3%; CE, 76.5 cd A^{-1}), indicating a near-perfect charge balance and superior outcoupling efficiency. In addition, the valley-centre tandem device showed a higher power efficiency of 80.8 lm W^{-1} compared with the single PeLED device (61.2 lm W^{-1}) and single OLED device (77.6 lm W^{-1}). (Fig. 2a–d, Supplementary Fig. 5a,b and Extended Data Table 1). This result is one of the highest efficiencies, which surpasses the highest device efficiency of single PeLEDs based on polycrystalline perovskites and colloidal PNCs, and this tandem device showed good reproducibility (Fig. 2e and Supplementary Fig. 5c). The wall-plug efficiency, which is the radiant power divided by the input electrical power during the operation of a device, was also increased in the h-tandem device to 14.5% from the wall-plug efficiency of 10.8% for the single PeLED device (Extended Data Table 1)[18]. The increased wall-plug efficiency combined with the narrow (27.3 nm) EL emission of the h-tandem device makes it perfectly applicable for energy-efficient and vivid next-generation displays. The h-tandem PeLED also showed high operating stability with a device lifetime of L_{50} = 113 h at L_0 = 1,000 cd m^{-2} of electrical stress, which corresponds to an estimated lifetime of 5,596 h at L_0 = 100 cd m^{-2} (Extended Data Fig. 1).

We performed a time-resolved EL analysis using a streak camera to investigate the turn-on and turn-off response characteristics of the h-tandem PeLED at the valley-centre structure (Fig. 2f–h and Supplementary Fig. 6). The EL onset time, which is defined as the time delay from the turn on of the pulse voltage, of the PeLED was shorter than that of the OLED due to the higher charge carrier mobility of perovskite emitters than that of organic emitters. However, the saturation time and turn-off decay time of the EL intensity in the PeLED were much delayed compared with those of the OLED due to ion migration and trapped charge carriers in perovskite emitters, as determined from the in-device time-resolved photoluminescence (PL) measurements (Supplementary Figs. 7 and 8). For valley-centre tandem, both turn-on and turn-off response times were improved compared with those of the OLED and PeLED, respectively (Fig. 2f). Furthermore, the time-resolved EL spectra of valley-centre tandem showed stable emission spectra from the beginning of device operation until 500 μs; this confirms that the perovskite and organic emitter simultaneously responded to the voltage pulse and uniformly contributed to the EL emission (Fig. 2g,h). In addition, the valley-centre tandem structure was successfully applied to a flexible large-area display with an area of 4 cm × 4 cm and a 10 × 10 passive matrix display (Fig. 2i).

Charge balance in h-tandem PeLED

In conventional tandem OLEDs stacked with the same type of emitting device with similar J–V–L characteristics, simply coupling two units nearly doubles the device efficiency without a large modification of

https://doi.org/10.1038/s41565-023-01581-2

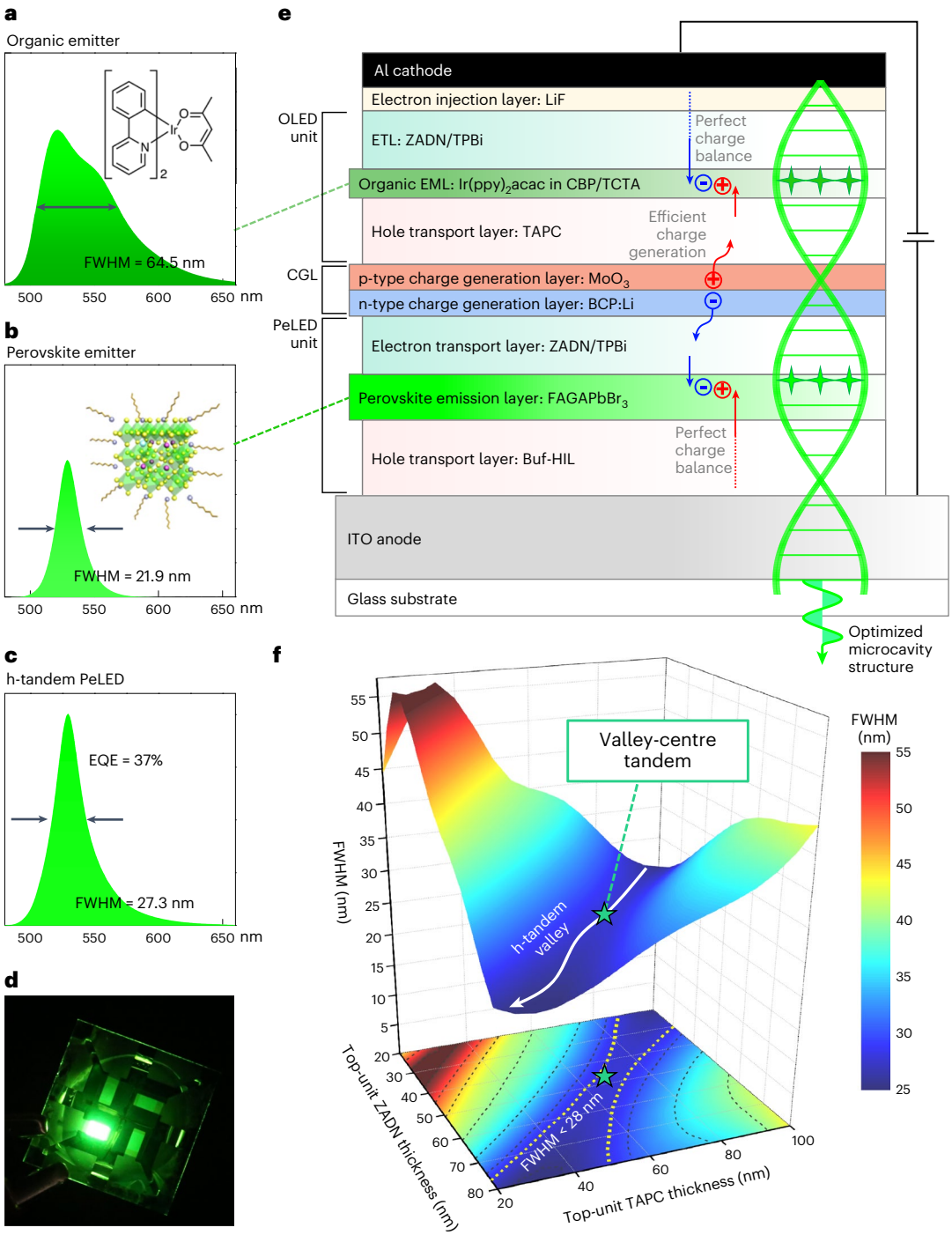

Fig. 1 | Concept of h-tandem PeLED and the crucial optical microcavity structure (h-tandem valley). a–**c**, EL spectra of OLED (**a**), PeLED (**b**) and h-tandem PeLED (**c**). **d**, Photograph of an operating h-tandem PeLED. **e**, Schematic of the device structure. **f**, Optical simulation of the FWHM of the h-tandem PeLED. Contour plots are the simulated FWHM depending on the thickness of ZADN and TAPC in the top unit. The h-tandem valley with FWHM narrower than 28 nm and valley-centre tandem (50 nm ZADN and 65 nm TAPC) are indicated.

the device structure (Supplementary Figs. 9 and 10 and Supplementary Table 1). In h-tandem PeLEDs, the component devices have different resistances and *J*–*V*–*L* characteristics so that the current flow from the CGL to each emitting unit can be unbalanced, which might lead to a loss of injected charges and a shift in the emission peak or broadened emission spectra arising from the unbalanced luminance of each unit. To promote balanced charge injection/transport that is required to achieve high device efficiency, we fabricated various devices with different ETLs (Fig. 3a and Supplementary Fig. 11a–d). In addition, we also fabricated single PeLEDs (separated bottom units) and single OLEDs (separated top units) with corresponding ETL structures for the bottom and top units in the tandem devices to compare the current densities of the bottom and top units. By introducing BCP:Li as the CGL and replacing the TPBi-BCP:Li interface with ZADN-BCP:Li, charge generation and electron injection became efficient due to the lowered electron injection barrier (Fig. 3a and Supplementary Figs. 11e–h, 12 and 13)[19]. In particular, in valley-centre tandem where the ETLs of both bottom and top units are replaced, the current density–voltage curves

https://doi.org/10.1038/s41565-023-01581-2

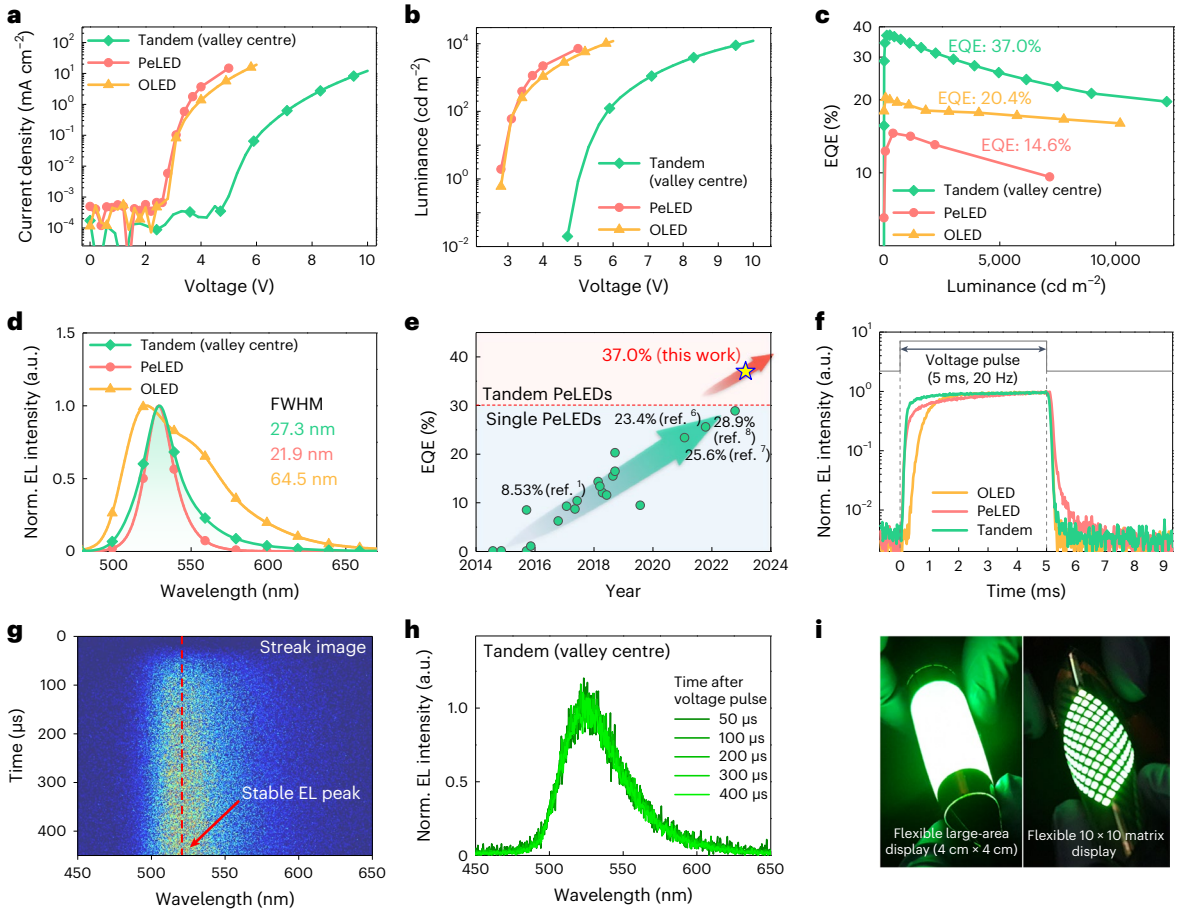

Fig. 2 | Device characteristics of the PeLED, OLED and h-tandem PeLED. **a**–**d**, Current density–voltage curve (**a**), luminance–voltage curve (**b**), EQE–luminance curve (**c**) and normalized EL spectra (**d**). **e**, Summary of the reported green PeLEDs on the basis of the maximum EQE. **f**, Transient EL intensity of the PeLED, OLED and h-tandem PeLED. **g**, Streak camera image of the h-tandem PeLED during turn on in the timescale of 500 μs. **h**, Time-resolved spectra of h-tandem PeLEDs during turn on in the timescale of 500 μs. **i**, Photographs of flexible h-tandem PeLEDs with an active area of 4 cm × 4 cm and a flexible large-area display with a 10 × 10 passive matrix display.

of the bottom and top units perfectly matched in the driving voltage of 2.6–3.2 V, where the single PeLED and single OLED device show the maximum EQEs (Fig. 3b). In addition, the capacitance–voltage characteristics confirmed that the electrical characteristics of the bottom and top units are similar and the light emission from both emitters ideally occurs at the same voltage (Supplementary Fig. 14). Due to the well-matched current densities of the bottom and top units, the sum of EL from each unit was maximized in the tandem device, leading to the highest device efficiency in valley-centre tandem with an EQE of 37.0%, whereas unbalanced tandem 1–3 showed lower EQEs of 25.8%, 26.4% and 21.0%, respectively, even though they had similar device structures (Fig. 3c–e, Supplementary Fig. 11i–l and Supplementary Table 2). In addition, the developed h-tandem PeLED that used ZADN for all ETLs (valley-centre tandem) had a stable EL peak position at 529 nm during operation, indicating that two EL units in the h-tandem PeLED stably contribute to the total EL spectrum, whereas unbalanced tandem 1–3 showed a shift and broadening in the EL spectra due to charge imbalance in each unit (Fig. 3g,h and Supplementary Fig. 15). The FWHM of the EL emission for valley-centre tandem was the narrowest for 27.3 nm, whereas those of unbalanced tandem 1–3 were 31.8, 28.4 and 42.2 nm (Supplementary Fig. 11k). The stable EL emission of valley-centre tandem is consistent with the simulated EL spectrum assuming perfect charge balance (Fig. 3i). This trend confirms that the perovskite and organic emitters emitted uniformly to form a narrow spectrum at only the valley-centre tandem structure. In addition, the response time of valley-centre tandem was reduced to 48 μs compared with the response time of 169 μs in unbalanced tandem 1 (Supplementary Fig. 16). The incorporation of h-tandem valley and its optimized thickness improved charge carrier injection into each unit and improved the charge balance in the top and bottom emitting units, which led to the fast response and stable luminance driving.

For the quantitative analysis of the charge balance, we performed an optical simulation of the tandem devices (Fig. 3f and Supplementary Fig. 11l). The EQEs calculated from the optical simulation assuming perfect charge balance were 35.2%, 36.4%, 35.8%, 37.1% for unbalanced tandem 1–3 and valley-centre tandem, respectively, all of which were similar due to the same total thickness of the ETL and similar refractive index of TPBi and ZADN in the wavelength range of EL emission (Supplementary Fig. 17). The ratio of the experimentally measured EQE to the simulated value was 99.7% for valley-centre tandem, achieving a theoretical EQE indicating a near-perfect charge balance of both units in the tandem device. On the other hand, they were 73%, 73% and 59% for unbalanced tandem 1–3, respectively, implying that a large amount of efficiency loss can stem from the charge imbalance. The EQE of a tandem device can be expressed as the following equation:

$$\mathrm{EQE} = \xi_{\mathrm{CGE}} \times \{\gamma_{\mathrm{CB,OLED}} \times \chi_{\mathrm{S/T,OLED}} \times \Phi_{\mathrm{PLQY,OLED}} \times \eta_{\mathrm{out,OLED}} + \gamma_{\mathrm{CB,PeLED}} \times \chi_{\mathrm{S/T,PeLED}} \times \Phi_{\mathrm{PLQY,PeLED}} \times \eta_{\mathrm{out,PeLED}}\},$$

where ξ_{CGE} is defined as the number of electrons (holes) generated at the CGL divided by the number of electrons (holes) injected from

https://doi.org/10.1038/s41565-023-01581-2

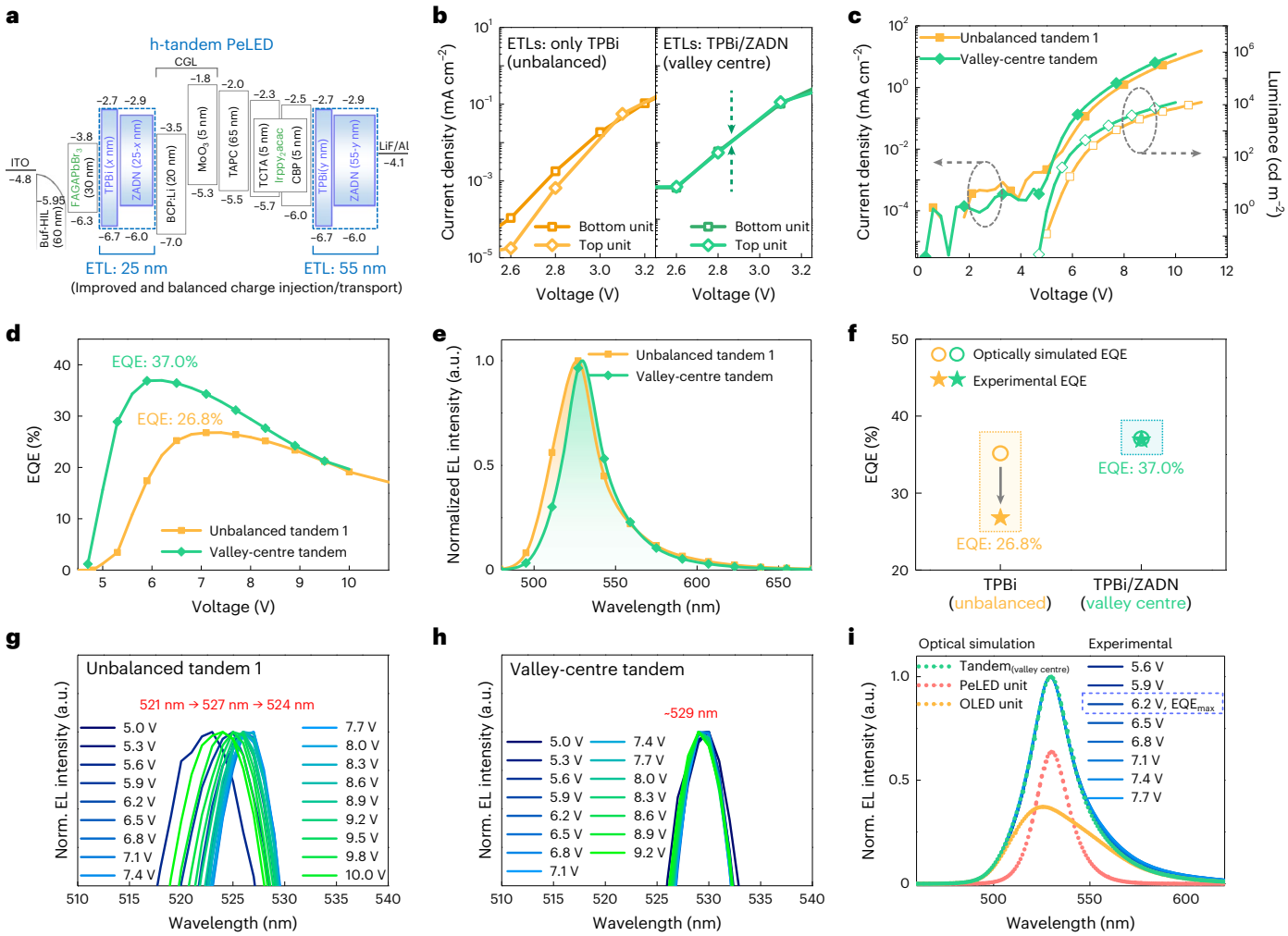

Fig. 3 | Electrical optimization of tandem devices by varying the ETLs of bottom and top units. a, Device structures of unbalanced tandem using only TPBi for the ETL ($x = 25$ nm, $y = 55$ nm) and valley-centre tandem using TPBi/ZADN for the ETL ($x = 5$ nm, $y = 5$ nm). **b**, Comparison of the current density–voltage curve of the single PeLED (bottom unit) and OLED (top unit). **c**–**e**, Device characteristics of unbalanced tandem and valley-centre tandem. Current density–voltage and luminance–voltage curves (**c**), EQE–voltage curves (**d**) and normalized EL spectra (**e**). **f**, Comparison of the EQEs calculated from the optical simulation assuming perfect charge balance and the experimental EQEs of the fabricated tandem devices. **g**,**h**, Shift in the EL peak position of unbalanced tandem 1 (**g**) and valley-centre tandem (**h**) at various driving voltages. **i**, Optical simulation of the EL spectra of valley-centre tandem compared with the EL spectra of the fabricated device at various driving voltages. The EL spectra were simulated assuming perfect charge balance in both PeLED unit and OLED unit. Total emission of the tandem device, emission from the PeLED unit and emission from the OLED unit are shown in the simulated EL spectra.

the electrode; γ_{CB} is the charge balance factor, that is, the number of generated excitons divided by the number of injected electrons (holes); $\chi_{S/T}$ is the radiative exciton ratio, which is 1 for both phosphorescent OLED and PeLED; Φ_{PLQY} is the photoluminescence quantum yield (PLQY) of the EML; and η_{out} is the outcoupling efficiency. Here γ_{CB} is a critical factor in analysing the discrepancy between the theoretical EQE and experimental EQE, and charge generation efficiency (ξ_{CGE}) is also an important factor in investigating the performance of CGLs[20,21]. To confirm the near-perfect charge balance in the tandem device, we simulated the EL spectrum assuming perfect charge balance in both PeLED and OLED units (Fig. 3i and Supplementary Fig. 18). The simulated EL spectrum was almost identical to the EL spectrum of the fabricated tandem device at the maximum EQE. Hence, the contributions of PeLED and OLED in the total emission of the fabricated tandem device were the same as those of the optical simulation assuming perfect charge balance, indicating that the charge balance of both units in the fabricated valley-centre tandem was also almost perfect. In addition, the charge balance of the h-tandem PeLED was also confirmed from the bias-dependent in-device time-resolved PL (Supplementary Fig. 8). Moreover, the EL spectra of the tandem device in the voltage range of 5.6–7.7 V were almost identical, indicating that the charge balance and contribution to the total EL emission of the PeLED and OLED units remains almost unchanged in this driving voltage range. Because the charge balances of each unit in the valley-centre tandem device is almost identical ($\gamma_{CB,1} = \gamma_{CB,2}$), we can calculate the product of the charge generation efficiency and charge balance factor, which results in the following:

$$\xi_{CGE} \times \gamma_{CB} = 37.0\%/37.1\% = 0.997\,(99.7\%).$$

This indicates that there is almost no loss of injected charges in valley-centre tandem.

Comprehensive electrical and optical analyses of h-tandem PeLEDs

Optically achievable efficiency is determined by the microcavity structure of the device. However, because varying the thickness of the hole transport layer and ETL also affects the charge balance, the maximum

https://doi.org/10.1038/s41565-023-01581-2

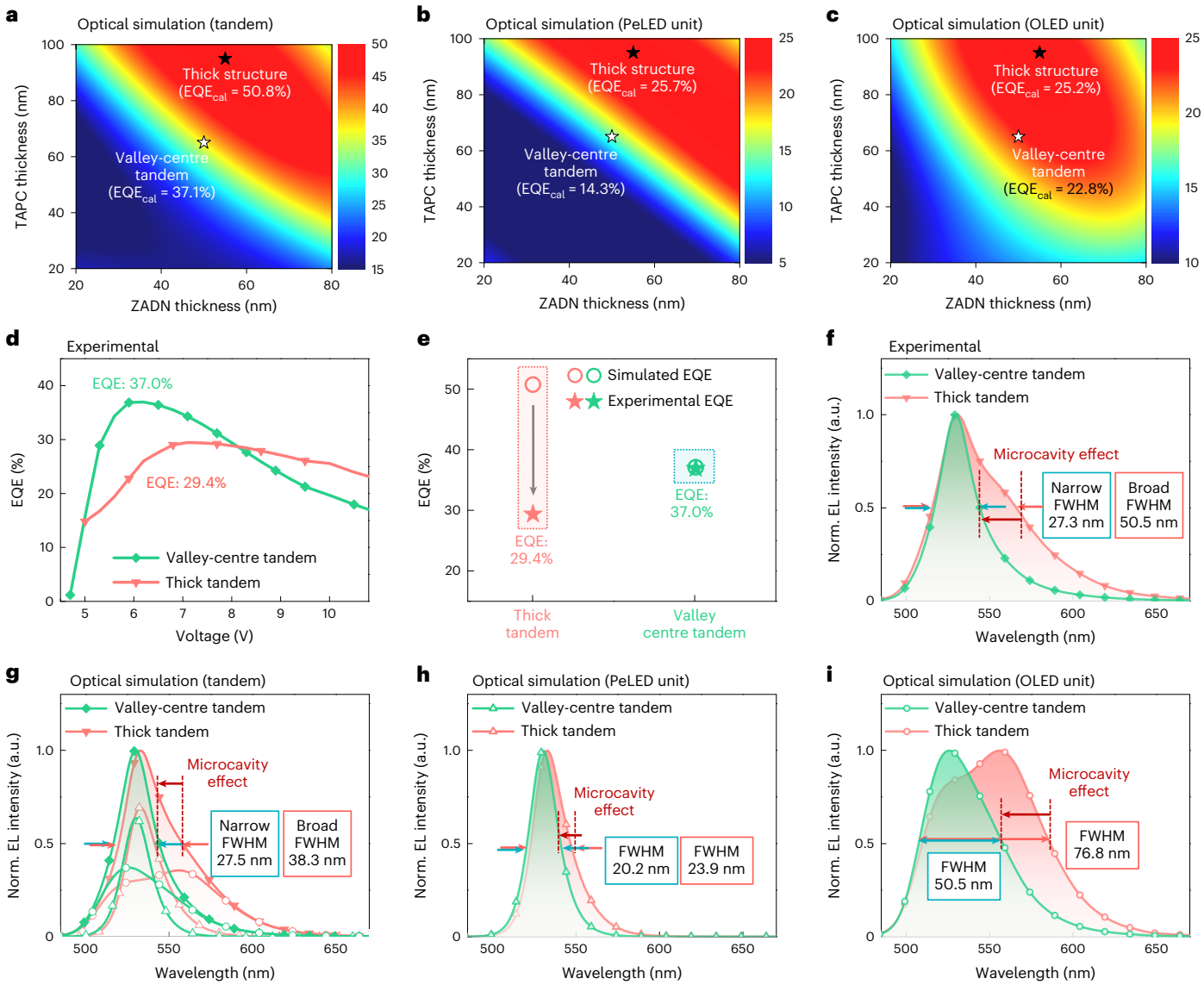

Fig. 4 | Optical simulation and device characteristics of valley-centre tandem and thick tandem. a–c, Optical simulation of the achievable EQEs of h-tandem PeLED (**a**), PeLED unit in h-tandem PeLED (**b**) and OLED unit in h-tandem PeLED (**c**) depending on the thickness of ZADN and TAPC in the OLED unit. Valley-centre tandem (optimal structure): TAPC 65 nm and ZADN 50 nm of OLED unit, best-performing structure. Thick tandem: TAPC 95 nm and ZADN 55 nm of OLED unit, optimized structure only for achieving the maximum outcoupling efficiency. **d–f**, Comparison of device characteristics of valley-centre tandem and thick tandem. EQE–voltage curve (**d**), comparison of experimental EQE and optically simulated EQE (**e**) and EL spectra of the fabricated tandem devices (**f**). **g–i**, Simulated EL spectra of h-tandem PeLED (**g**), PeLED unit (**h**) and OLED unit (**i**) for valley-centre tandem and thick tandem devices. In **g**, the contribution of the PeLED unit (hollow triangle symbol) and OLED unit (hollow circle symbol) to the total emission of the tandem device are shown. The optical simulations were performed assuming no electrical loss in the device, that is, ideal charge balance in the device.

outcoupling device structure obtained from the optical simulation does not always result in the highest device efficiency. For the comprehensive electrical and optical analyses, we performed an optical simulation of the EQE and EL spectra depending on the thickness of ZADN and TAPC in the top unit, and compared the simulation results with the experimental EL characteristics of valley-centre tandem and the device with a thick structure for the maximum outcoupling efficiency (thick tandem) (Fig. 4a–c, Supplementary Figs. 19–21 and Supplementary Table 3). For valley-centre tandem, the theoretical EQE from the optical simulation was 37.1%. For thick tandem, the theoretical EQE only from the optical simulation without considering the charge balance was 50.8%. However, the experimental EQE of the fabricated thick tandem was only 29.4%, which was much lower than the calculated EQE from the optical simulation of thick tandem (50.8%) as well as the experimental EQE of valley-centre tandem (37.0%) (Fig. 4d,e and Supplementary Fig. 22). This indicates that there is a large amount of electrical loss due to the charge imbalance in thick tandem, whereas there is almost no electrical loss in valley-centre tandem with near-perfect charge balance (close to 100%) (Fig. 4e). In addition, the thick tandem showed broad emission with an FWHM of 50.5 nm, whereas valley-centre tandem showed narrow emission with an FWHM of 27.3 nm (Fig. 4f). As shown in the simulated EL spectrum, thick tandem showed much broader FWHM for 38.3 nm due to the spectrum-shaping effect of the microcavity (Fig. 4g–i and Supplementary Figs. 2 and 3). In particular, the shoulder peak (556 nm) of the OLED unit becomes stronger than the first peak (526 nm) due to the lengthened microcavity structure, leading to a broad FWHM (Fig. 4i). Consequently, the colour coordinates of thick tandem (0.328, 0.641) are inferior to those of valley-centre tandem (0.223, 0.720).

Not only the thickness of the transporting layers in the top unit but also the thickness of the transporting layers in the bottom unit

https://doi.org/10.1038/s41565-023-01581-2

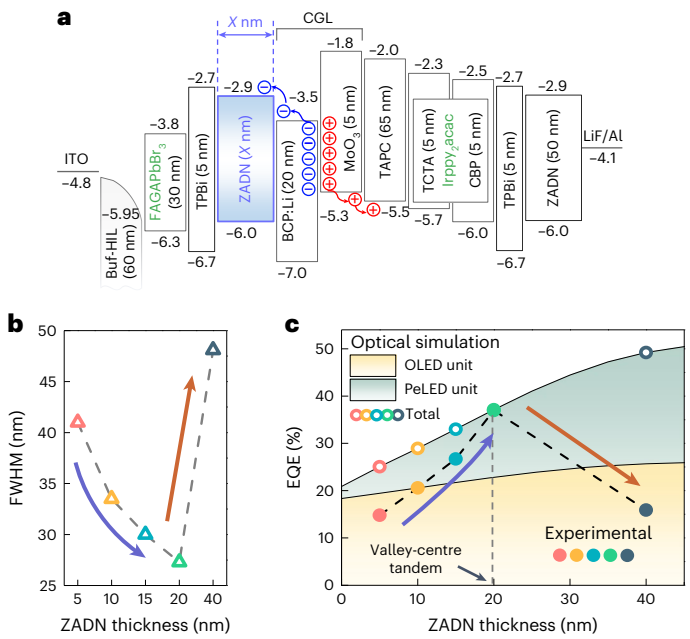

Fig. 5 | Electrical and optical optimizations of h-tandem PeLED by varying the ZADN (ETL) thickness of the PeLED unit in the tandem device. a, Device structure shown along with the charge generation process. The ZADN layer (X = 5, 10, 15, 20 and 40 nm) in the PeLED is indicated in the device structure. **b**, FWHM of the h-tandem PeLED with various ZADN thicknesses in the PeLED unit. **c**, Optical simulation of the h-tandem PeLED compared with the experimental EQEs. The solid and hollow circles indicate the experimental EQE and simulated EQE, respectively.

affect the microcavity structure of the tandem device. In addition, since the ZADN ETL of the bottom unit is adjacent to the BCP:Li CGL, its thickness is critical to the charge generation efficiency and charge balance factor. Hence, we also performed comprehensive electrical and optical analyses by varying the thickness of ZADN in the bottom unit from 5 to 40 nm (Fig. 5 and Supplementary Fig. 23). The EL spectrum of valley-centre tandem shows the narrowest bandwidth among the tandem devices with various ZADN thicknesses, indicating that the microcavity effect is optimal at a ZADN thickness of 20 nm for high colour purity (Fig. 5b). The optically calculated EQE increases with the increase in ZADN thickness from 5 to 20 nm. Meanwhile, the gap between the EQE from optical simulation and the EQE of the fabricated tandem device decreases with an increase in the ZADN thickness, becoming almost identical at a ZADN thickness of 20 nm (h-tandem valley) (Fig. 5c). The charge balance factor of the tandem device was the highest for 99.7% at the bottom unit for a ZADN thickness of 20 nm (valley-centre tandem), and the devices with a ZADN thinner or thicker than 20 nm showed lower charge balances. Consequently, the EQE of the fabricated tandem devices was the highest at a ZADN thickness of 20 nm (valley-centre tandem). The increase in the ZADN thickness from 5 to 20 nm leads to an increase in the charge balance factor as well as outcoupling efficiency. In addition, the optical simulation shows that the total outcoupling efficiency increases with the ZADN thickness in the PeLED unit (Fig. 5c). However, the fabricated device with a thicker ZADN (thickness, 40 nm) shows a decreased EQE of 15.9% even though the calculated outcoupling efficiency is near 50.0%, indicating a drop in the charge balance factor. Hence, the optimal device structure for the maximum outcoupling efficiency does not guarantee the maximum EQE of a real h-tandem PeLED. Based on the comprehensive electrical and optical analyses, we found that the h-tandem PeLED structure of the valley-centre tandem was optimal for the EQE and narrowband emission.

Conclusion

We developed an optical and electrical design strategy to realize vivid and efficient h-tandem PeLEDs by combining a thin and transparent colloidal nanocrystal PeLED unit with an OLED unit that provides a more favourable display-manufacturing process. Through the design of an optical valley for the optimal microcavity effect and charge balance, we finely matched the current level and achieved a near-perfect charge balance in tandem devices. As a result, the h-tandem PeLED with a high device efficiency (CE = 151.8 cd A^{-1}; EQE = 37.0%) and a narrow FWHM of 27.3 nm were achieved. In addition, the optical simulation revealed how the device structure affects the microcavity structure and charge balance in the tandem device that results in different EL spectra and EQEs, and finally verified that our h-tandem PeLED at the h-tandem valley has a well-designed device structure both electrically and optically. Our experimental results and comprehensive electrical and optical investigations present a guideline and insights into further development of h-tandem displays incorporating different types of emitting unit such as PeLEDs, OLEDs and quantum dot LEDs, leading to commercially viable next-generation displays that can achieve high efficiency and high colour reproducibility.

Online content

Any methods, additional references, Nature Portfolio reporting summaries, source data, extended data, supplementary information, acknowledgements, peer review information; details of author contributions and competing interests; and statements of data and code availability are available at https://doi.org/10.1038/s41565-023-01581-2.

References

1. Cho, H. et al. Overcoming the electroluminescence efficiency limitations of perovskite light-emitting diodes. *Science* **350**, 1222–1225 (2015).
2. Kim, Y.-H. et al. Multicolored organic/inorganic hybrid perovskite light-emitting diodes. *Adv. Mater.* **27**, 1248–1254 (2015).
3. Protesescu, L. et al. Nanocrystals of cesium lead halide perovskites ($CsPbX_3$, X=Cl, Br, and I): novel optoelectronic materials showing bright emission with wide color gamut. *Nano Lett.* **15**, 3692–3696 (2015).
4. Kim, Y.-H., Cho, H. & Lee, T.-W. Metal halide perovskite light emitters. *Proc. Natl Acad. Sci. USA* **113**, 11694–11702 (2016).
5. Quan, L. N. et al. Perovskites for next-generation optical sources. *Chem. Rev.* **119**, 7444–7477 (2019).
6. Kim, Y.-H. et al. Comprehensive defect suppression in perovskite nanocrystals for high-efficiency light-emitting diodes. *Nat. Photon.* **15**, 148–155 (2021).
7. Ma, D. et al. Distribution control enables efficient reduced-dimensional perovskite LEDs. *Nature* **599**, 594–598 (2021).
8. Kim, J. S. et al. Ultra-bright, efficient and stable perovskite light-emitting diodes. *Nature* **611**, 688–694 (2022).
9. Woo, S.-J., Kim, J. S. & Lee, T.-W. Characterization of stability and challenges to improve lifetime in perovskite LEDs. *Nat. Photon.* **15**, 630–634 (2021).
10. Fan, X. C. et al. Ultrapure green organic light-emitting diodes based on highly distorted fused π-conjugated molecular design. *Nat. Photon.* **17**, 280–285 (2023).
11. Chen, Y. et al. Approaching nearly 40% external quantum efficiency in organic light emitting diodes utilizing a green thermally activated delayed fluorescence emitter with an extended linear donor–acceptor–donor structure. *Adv. Mater.* **33**, 2103293 (2021).
12. Han, T.-H. et al. Approaching ultimate flexible organic light-emitting diodes using a graphene anode. *NPG Asia Mater.* **8**, e303 (2016).

13. Chang, Y. W. et al. A versatile ferrocene-containing material as a p-type charge generation layer for high-performance full color tandem OLEDs. *Chem. Commun.* **52**, 14294–14297 (2016).
14. Cho, T. Y., Lin, C. L. & Wu, C. C. Microcavity two-unit tandem organic light-emitting devices having a high efficiency. *Appl. Phys. Lett.* **88**, 111106 (2006).
15. Wang, L. et al. Design of high-performance tandem blue devices for quantum-dot OLED display. *SID Symp. Dig. Tech. Pap.* **51**, 929–932 (2020).
16. Mizusaki, M. et al. Single and tandem OLED display technologies with high efficiency and long lifetime. *SID Symp. Dig. Tech. Pap.* **52**, 278–281 (2021).
17. Chan, C. Y. et al. Stable pure-blue hyperfluorescence organic light-emitting diodes with high-efficiency and narrow emission. *Nat. Photon.* **15**, 203–207 (2021).
18. Forrest, S. R., Bradley, D. D. C. & Thompson, M. E. Measuring the efficiency of organic light-emitting devices. *Adv. Mater.* **15**, 1043–1048 (2003).
19. Sun, Y. et al. Improved performance of red phosphorescent organic light emitting diodes using partial mixed host system. *J. Nanosci. Nanotechnol.* **15**, 8081–8085 (2015).
20. Kim, J. M., Lee, C. H. & Kim, J.-J. Mobility balance in the light-emitting layer governs the polaron accumulation and operational stability of organic light-emitting diodes. *Appl. Phys. Lett.* **111**, 203301 (2017).
21. Kröger, M. et al. Temperature-independent field-induced charge separation at doped organic/organic interfaces: experimental modeling of electrical properties. *Phys. Rev. B* **75**, 235321 (2007).

Methods

Materials

Materials for synthesis: oleic acid (90.0%, Alfa Aesar), *n*-decylamine (98.0%, TCI), guanidinium bromide (GABr, >99%, GreatCell Solar), formamidinium bromide (FABr, >99.99%, GreatCell Solar), lead(II) bromide ($PbBr_2$, 99.999%, Sigma-Aldrich), toluene (99.5%, Samchun Chemicals), 1-butyl alcohol (99.0%, Samchun Chemicals), *N*,*N*-dimethylformamide (>99.8%, Sigma-Aldrich). All chemicals listed above were used without any further treatment.

Materials for thermally deposited layer: molybdenum oxide (MoO_3, 99.97%) and lithium nitride (Li_3N, ≥99.50%) were purchased from Sigma-Aldrich. Also, 2-[4-(9,10-di-naphthalen-2-yl-anthracen-2-yl)-phenyl]-1-phenyl-1H-benzoimidazole (ZADN, >99%) was purchased from Suzhou Geao New Material. Bathocuproine (BCP), 2,2′,2″-(1,3,5-benzinetriyl)-tris(1-phenyl-1H-benzimidazole) (TPBi, >99.9%), 1,1-bis[(di-4-tolylamino)phenyl]cyclohexane (TAPC, >99.9%), tris(4-carbazoyl-9-ylphenyl)amine (TCTA, >99.9%), 4,4′-bis(N-carbazolyl)-1,1′-biphenyl (CBP, >99.9%) and bis(2-phenylpyridine) iridium(III) acetylacetonate ($Ir(ppy)_2acac$, >99.5%) were purchased from OSM. Lithium fluoride was purchased from Foosung.

Synthesis of PNC

$FA_{0.9}GA_{0.1}PbBr_3$ PNCs were synthesized in air at room temperature (17–19 °C). Precursor solution, prepared in accordance with our previous report[6] with slight modifications, was formulated by dissolving FABr, GABr and $PbBr_2$ (with the FABr:GABr ratio maintained at 9:1 and the molarities of FABr+GABr and $PbBr_2$ maintained at 0.2 and 0.1 mmol, respectively) in 0.5 ml anhydrous *N*,*N*-dimethylformamide. Then, 0.15 ml of the precursor solution was dropped into a crystallization-inducing solution comprising 5.00 ml of toluene, 2.00 ml of 1-butanol, 0.30 ml of oleic acid and 24.2 µl of *n*-decylamine, which was mixed for 10 min under vigorous stirring. The resulting colloidal PNCs were washed by sequential centrifugation and then collected in toluene.

Fabrication of h-tandem PeLED

Indium tin oxide patterned glasses were cleaned by sequential sonication in acetone and 2-propanol for 15 min each. The glasses were boiled in 2-isopropanol for 5 min, then transferred into an ultraviolet–ozone cleaner and treated with ultraviolet–ozone for 10 min to remove the residual organics. A buffered hole injection layer (Buf-HIL) composed of poly(3,4-ethylenedioxythiophene)/poly(styrene sulfonate) and perfluorinated ionomer were then spin coated in air, which was then annealed at 150 °C for 30 min for the effective self-organization of pol y(3,4-ethylenedioxythiophene)/poly(styrene sulfonate) and perfluorinated ionomer[22,23]. For the flexible device, we annealed the Buf-HIL at 80 °C for 30 min due to the low glass transition temperature (T_g) of the polyethylene terephthalate substrate (~85 °C). The samples were then transferred into a glove box, in which the emitting layers were formed by spin-coating $FA_{0.9}GA_{0.1}PbBr_3$ PNC solutions at 500 r.p.m. for 60 s. The 1,3,5-tris(bromomethyl)−2,4,6-triethylbenzene solutions, which were dissolved in toluene, were spin coated at 3,000 r.p.m. for 60 s for forming the insulating interlayer, which can improve the charge balance. The samples were transferred to a vacuum evaporator, and then a 5-nm-thick layer of TPBi, 20-nm-thick layer of ZADN, 20-nm-thick co-deposited layer of BCL:Li (9:1 vol%), 5-nm-thick layer of MoO_3, 65-nm-thick layer of TAPC, 5-nm-thick layer of a co-deposited layer of TCTA:$Ir(ppy)_2acac$ (97:3 vol%), 5-nm-thick co-deposited layer of CBP:$Ir(ppy)_2acac$ (96:4 vol%), 5-nm-thick layer of TPBi, 50-nm-thick layer of ZADN, 1-nm-thick layer of lithium fluoride and 100-nm-thick layer of aluminium were sequentially deposited. Single PeLED structure is shown in supporting material, distinguishing from our previously reported PeLED[6] due to the modified ETL. All the samples were encapsulated before the measurements.

EL measurement

The *J*–*V*–*L* characteristics of the LEDs were measured using a Keithley 236 source measure unit and a Minolta CS 2000 spectroradiometer. The EQE of the h-tandem PeLED was calculated by measuring the full angular EL distribution[24].

Capacitance–voltage analysis

Capacitance–voltage characteristics were measured using electrochemical impedance spectroscopy (Biologic, SP-200). All the devices were measured over a voltage range of 0 to 10 V at a constant frequency (1,000 Hz) in the dark state.

Transient EL measurement

Transient EL and time-resolved spectra were obtained using a system composed of a streak camera (C10627, Hamamatsu Photonics), a delay generator (DG645, Stanford Research Systems) and a function generator (Agilent 33250A). A voltage pulse with 5 ms width, 20 Hz repetition rate and a voltage around the turn-on voltage of each device (OLED and PeLED, 3.0 V; tandem LED, 5.9 V) was used.

Transient PL measurement

Transient PL decay and time-resolved spectra of the perovskite/organic thin films and in-device transient PL measurements were carried out with a system composed of a streak camera (C10627, Hamamatsu Photonics), a delay generator (DG645, Stanford Research Systems) and a nitrogen pulse laser (337 nm, 20 Hz, Usho Optical Systems).

Optical simulation

Optical simulations were calculated using a code based on the classical dipole model and an optical simulation software package (J-OSTD, JooAm), which is based on the aforementioned code[25–28]. The input parameters for the simulations included the refractive indices of the layers, PLQY and PL spectra of the EMLs, emitting dipole orientations of the EMLs and the emission-zone distribution of the EMLs obtained from the experiments described below. The refractive indices of the organic layers were obtained from the optical fitting of the variable-angle spectroscopic ellipsometry data (angles 50–70°), measured with a variable-angle spectroscopic ellipsometer (J.A. Woollam M-2000). Photon recycling in the perovskite EML was not considered, as it is very thin (30 nm)[29].

The emission zone of each unit in the tandem device was determined by comparing the angle-dependent EL intensity obtained from the experimental measurement and optical simulation (Supplementary Fig. 19). The emission zone of the PeLED unit and OLED unit were determined to be 30 nm (edge to the ETL side) and 5 nm (middle of the EML), respectively. The film PLQY of $Ir(ppy)_2acac$ and PNC were measured to be 86% and 77%, respectively. The emitting dipole orientations of $Ir(ppy)_2acac$ and PNC were determined to be 74.0% and 66.7% (isotropic), respectively, from the angle-dependent PL intensity analysis (Supplementary Fig. 24). For the PLQY measurements, perovskite and organic EMLs were prepared on bare quartz substrates via spin coating and vacuum evaporation, respectively. For the optical simulation of the tandem device, two EMLs (top and bottom) were inserted in the device model. All the simulations were performed assuming perfect charge balance in both bottom and top units, which means that the number of electrically generated excitons was the same for both units. The simulated EL spectra and FWHM of the devices included in the main text are from the simulated EL spectra at a forward viewing angle (0°), as the forward viewing angle best represents the spectrum of the tandem device (Supplementary Figs. 19, 20 and 25). The optical simulation itself considers the Purcell effect. Therefore, the calculated EQE from the optical simulation can be represented as $EQE_{sim} = \int PLQY_{eff}(\lambda) \times \eta_{out}(\lambda) d\lambda$, where $PLQY_{eff}(\lambda)$ is the effective PLQY determined by the Purcell effect and $\eta_{out}(\lambda)$ is the outcoupling efficiency at a given wavelength λ.

Data availability

The data that support the findings of this study are available from the corresponding author upon reasonable request.

References

22. Lee, T.-W., Chung, Y., Kwon, O. & Park, J. J. Self-organized gradient hole injection to improve the performance of polymer electroluminescent devices. *Adv. Funct. Mater.* **17**, 390–396 (2007).
23. Han, T.-H. et al. Extremely efficient flexible organic light-emitting diodes with modified graphene anode. *Nat. Photon.* **6**, 105–110 (2012).
24. Jeong, S.-H. et al. Characterizing the efficiency of perovskite solar cells and light-emitting diodes. *Joule* **4**, 1206–1235 (2020).
25. Furno, M., Meerheim, R., Hofmann, S., Lüssem, B. & Leo, K. Efficiency and rate of spontaneous emission in organic electroluminescent devices. *Phys. Rev. B* **85**, 115205 (2012).
26. Moon, C.-K., Kim, S.-Y., Lee, J.-H. & Kim, J.-J. Luminescence from oriented emitting dipoles in a birefringent medium. *Opt. Express* **23**, A279–A291 (2015).
27. Kim, K. H. et al. Phosphorescent dye-based supramolecules for high-efficiency organic light-emitting diodes. *Nat. Commun.* **5**, 4769 (2014).
28. Lee, J. et al. Synergetic electrode architecture for efficient graphene-based flexible organic light-emitting diodes. *Nat. Commun.* **7**, 11791 (2016).
29. Cho, C. et al. The role of photon recycling in perovskite light-emitting diodes. *Nat. Commun.* **11**, 611 (2020).
30. Zou, Y. et al. High-performance narrowband pure-red OLEDs with external quantum efficiencies up to 36.1% and ultralow efficiency roll-off. *Adv. Mater.* **34**, 2201442 (2022).

Acknowledgements

This work was supported by the National Research Foundation of Korea (NRF) grant Brain Link program (2022H1D3A3A01081288) and the NRF grant funded by the Korea government (Ministry of Science and ICT) (NRF-2016R1A3B1908431, 2022M3H4A1A04096380).

Author contributions

H.-D.L., S.-J.W. and T.-W.L. conceived the research idea. H.-D.L. and S.K. fabricated the devices. S.-J.W. performed the optical simulation and optical and photophysical analyses of the devices. S.-J.W., H.-D.L. and J.P. performed the transient EL measurement of the devices. S.-J.W. and H.-D.L. performed the electrical analysis of the devices. S.K. synthesized the nanocrystals. S.-J.W., J.K. and S.Y. discussed the optical simulation results. H.-D.L. measured the *J*–*V*–*L* data of the devices. H.Z., S.J.H. and H.-D.L. fabricated the flexible LED devices. S.-J.W., K.Y.J. and D.-H.K. performed the transient PL measurements of the thin-film samples. S.-J.W., H.-D.L., S.K. and T.-W.L. wrote the paper. All authors contributed to the final paper. T.-W.L. supervised the research project.

Competing interests

The authors declare no competing interests.

Additional information

Extended data is available for this paper at https://doi.org/10.1038/s41565-023-01581-2.

Supplementary information The online version contains supplementary material available at https://doi.org/10.1038/s41565-023-01581-2.

Correspondence and requests for materials should be addressed to Tae-Woo Lee.

Peer review information *Nature Nanotechnology* thanks Cuong Dang, Biwu Ma and Jingbi You for their contribution to the peer review of this work.

https://doi.org/10.1038/s41565-023-01581-2

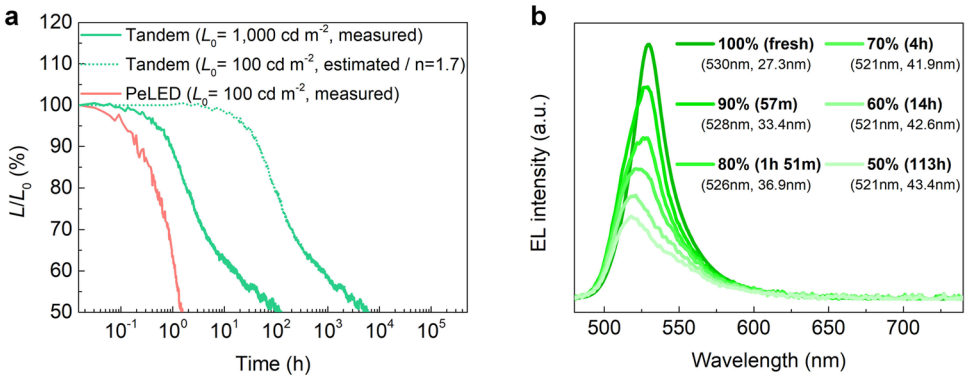

Extended Data Fig. 1 | Device lifetime characteristics of PeLED and hybrid tandem PeLED. a, The device lifetime of PeLED and hybrid tandem PeLED. The hybrid tandem PeLED showed device lifetime LT_{50} = 113 hours at L_0 = 1,000 cd m^{-2} of electrical stress which corresponds to estimated lifetime of 5,596 hours at L_0 = 100 cd m^{-2} using common acceleration factor of n = 1.7[8,30], whereas the single PeLED showed very short device lifetime (LT_{50} = 1 hour 48 min) at L_0 = 100 cd m^{-2}. **b**, EL spectra of hybrid tandem PeLED as a function of operating time at L_0 = 1,000 cd m^{-2}.

https://doi.org/10.1038/s41565-023-01581-2

Extended Data Table 1 | Device performance of single PeLED, single OLED, and hybrid tandem PeLED

Device	Current Efficiency (cd A^{-1})	Power Efficiency (lm W^{-1})	Wall Plug Efficiency (W/W, %)	EQE (%)	Luminance (cd m^{-2})	FWHM (nm)
Single PeLED	66.2	61.2	10.8	14.6	8,015	21.9
Single OLED	76.5	77.6	14.8	20.3	109,072	64.5
Hybrid tandem PeLED	151.8	80.8	14.5	37.0	28,579	27.3